ORIGINAL ARTICLE

Human biodistribution and radiation dosimetry of novel PET probes targeting the deoxyribonucleoside salvage pathway

Johannes Schwarzenberg · Caius G. Radu · Matthias Benz · Barbara Fueger ·
Andrew Q. Tran · Michael E. Phelps · Owen N. Witte · Nagichettiar Satyamurthy ·
Johannes Czernin · Christiaan Schiepers

Abstract

Purpose Deoxycytidine kinase (dCK) is a rate-limiting enzyme in deoxyribonucleoside salvage, a metabolic pathway involved in the production and maintenance of a balanced pool of deoxyribonucleoside triphosphates (dNTPs) for DNA synthesis. dCK phosphorylates and therefore activates nucleoside analogs such as cytarabine, gemcitabine, decitabine, cladribine, and clofarabine that are used routinely in cancer therapy. Imaging probes that target dCK might allow stratifying patients into likely responders and nonresponders with dCK-dependent prodrugs. Here we present the biodistribution and radiation dosimetry of three fluorinated dCK substrates, ^{18}F-FAC, L-^{18}F-FAC, and L-^{18}F-FMAC, developed for positron emission tomography (PET) imaging of dCK activity in vivo.

Methods PET studies were performed in nine healthy human volunteers, three for each probe. After a transmission scan, the radiopharmaceutical was injected intravenously and three sequential emission scans acquired from the base of the skull to mid-thigh. Regions of interest encompassing visible organs were drawn on the first PET scan and copied to the subsequent scans. Activity in target organs was determined and absorbed dose estimated with OLINDA/EXM. The standardized uptake value was calculated for various organs at different times.

Results Renal excretion was common to all three probes. Bone marrow had higher uptake for L-^{18}F-FAC and L-^{18}F-FMAC than ^{18}F-FAC. Prominent liver uptake was seen in L-^{18}F-FMAC and L-^{18}F-FAC, whereas splenic activity was highest for ^{18}F-FAC. Muscle uptake was also highest for ^{18}F-FAC. The critical organ was the bladder wall for all three probes. The effective dose was 0.00524, 0.00755, and 0.00910 mSv/MBq for ^{18}F-FAC, L-^{18}F-FAC, and L-^{18}F-FMAC, respectively.

Conclusion The biodistribution of ^{18}F-FAC, L-^{18}F-FAC, and L-^{18}F-FMAC in humans reveals similarities and differences. Differences may be explained by different probe affinities for nucleoside transporters, dCK, and catabolic enzymes such as cytidine deaminase (CDA). Dosimetry demonstrates that all three probes can be used safely to image the deoxyribonucleoside salvage pathway in humans.

Keywords Deoxyribonucleoside salvage pathway ·
Deoxycytidine kinase · PET imaging · FAC PET · Dosimetry

J. Schwarzenberg · M. Benz · B. Fueger · J. Czernin ·
C. Schiepers (✉)
Department of Molecular and Medical Pharmacology,
Ahmanson Biological Imaging Division,
David Geffen School of Medicine, University of California,
Los Angeles, CA, USA
e-mail: cschiepers@mednet.ucla.edu

J. Schwarzenberg
Department of Pediatrics, Medical University of Vienna,
Waehringer Guertel 18-20,
1090, Vienna, Austria

C. G. Radu · A. Q. Tran · M. E. Phelps · N. Satyamurthy
Department of Molecular and Medical Pharmacology,
Crump Institute for Molecular Imaging,
David Geffen School of Medicine, University of California,
Los Angeles, CA, USA

O. N. Witte
Howard Hughes Medical Institute and Department of
Microbiology, Immunology, and Molecular Genetics,
David Geffen School of Medicine, University of California,
Los Angeles, CA 90095, USA

Introduction

Positron emission tomography (PET) and PET/CT imaging using the glucose analog ^{18}F-fluorodeoxyglucose (FDG) are increasingly used to monitor the effects of cancer therapies. Treatment responders determined by FDG PET/CT have better overall survival rates than nonresponders [1]. However, cancer mortality, with few notable exceptions, has remained high implying that treatment response rates have not increased significantly [2]. One reason for the low response rates is the inability to measure molecular determinants of response that would allow clinicians to stratify cancer patients and therefore apply the most appropriate treatments.

Deoxycytidine kinase (dCK) is an attractive imaging and therapeutic target. dCK is a key enzyme in deoxyribonucleoside salvage, a biosynthetic pathway involved in production and maintenance of a balanced pool of deoxyribonucleoside triphosphates (dNTPs) for DNA synthesis (reviewed in [3]). dCK is highly expressed in hematopoietic/lymphoid cells, in lymphoid malignancies, and in some solid tumors (reviewed in [3]). Several prodrugs routinely used in cancer therapy such as cytarabine, gemcitabine [4, 5], decitabine, cladribine, and clofarabine [6] (Fig. 1a, b) require phosphorylation by dCK for their pharmacodynamic effects. As of November 2009 more than 1,000 clinical trials evaluating responses to such prodrugs were ongoing (Fig. 1b). However, response rates to these prodrugs are generally low, ranging from 5 to 30% and side effects can be severe. It would therefore be highly desirable to identify patients who are more likely to respond to treatment with these nucleoside analogs prior to therapy. This is, however, currently impossible.

Previously, we described the synthesis of the deoxycytidine analog ^{18}F-1-(2′-deoxy-2′-fluoro-arabinofuranosyl)cytosine (^{18}F-FAC) [7]. In subsequent work we showed that ^{18}F-FAC is a high affinity substrate for dCK [8]; this substrate is phosphorylated and trapped in tissues by this rate-limiting enzyme in the deoxyribonucleoside salvage pathway. ^{18}F-FAC and dCK-dependent prodrugs share the same biochemical pathway in cancer cells (Fig. 1a). Thus, ^{18}F-FAC PET may enable stratification of patients into likely responders versus poor or nonresponders to these prodrugs.

Deamination is one of the most important resistance mechanisms that explain the low response rates to some of the dCK-dependent prodrugs. Cytarabine, gemcitabine, and decitabine undergo extensive deamination in vivo by cytidine deaminase (CDA), an enzyme that is expressed at high levels in normal tissues and can be upregulated in tumors [9]. Deamination converts these prodrugs to inactive analogs. To circumvent the deamination problem, and thus increase drug effectiveness, purine nucleoside analogs such as cladribine and clofarabine have been developed [10]. Analogous to cytarabine, gemcitabine, and decitabine, ^{18}F-

FAC also undergoes deamination by CDA [11]. Deamination by CDA may affect the specificity of the PET dCK assay by producing a metabolite of ^{18}F-FAC that is not a substrate for dCK and thus may confound dCK imaging. Data in mice show that as early as 1 min after i.v. injection, ~14% of ^{18}F-FAC has been deaminated, and at 30 min post-injection, the vast majority (~90%) of ^{18}F-FAC has undergone deamination [11]. Deamination is likely to be even faster in humans, who express significantly more deaminase activity than mice [12].

To overcome the deamination problem and increase the metabolic stability of the probe, we have produced a series of deoxycytidine analogs that have high affinity for dCK, but are not susceptible to deamination. The rationale for developing these second-generation dCK-specific probes was that while dCK lacks stereospecificity and acts on both D- (natural) and L- (non-natural) substrate enantiomers [13], CDA is stereospecific and preferentially acts on natural nucleosides in the D-chiral conformation [13]. The production and preclinical characterization of radiolabeled L-enantiomers of ^{18}F-FAC are described elsewhere [11]. In this study we present the human biodistribution and radiation dosimetry of ^{18}F-FAC and of two non-natural deoxycytidine analogs, L-^{18}F-FAC [1-(2′-deoxy-2′-^{18}F-fluoro-arabinofuranosyl)cytosine] and L-^{18}F-FMAC (2′-deoxy-2′-^{18}F-fluoro-5-methyl-beta-L-arabinofuranosylcytosine). We also present initial PET images obtained with ^{18}F-FAC in a patient with lymphoma and with L-^{18}F-FMAC in a patient with metastatic ovarian cancer.

Materials and methods

Probes

Radiochemical synthesis, chemical and radiochemical quality control, i.e., radionuclide analysis, GC analysis for residual solvents, the test for Kryptofix, the test for pH, and the sterility and pyrogenicity tests, are described in the "Supplementary methods" section.

Human subjects

The study protocol was approved by the Institutional Review Board for Human Subjects at UCLA, the UCLA Medical Radiation Safety Committee, and the Radioactive Drug Research Committee (RDRC) of the US Food and Drug Administration (FDA). All human subjects provided written informed consent following a thorough explanation of the study by a qualified physician. Nine healthy volunteers (four women and five men with a median age of 26 years; range 21–34 years), one lymphoma patient, and one ovarian cancer patient were enrolled.
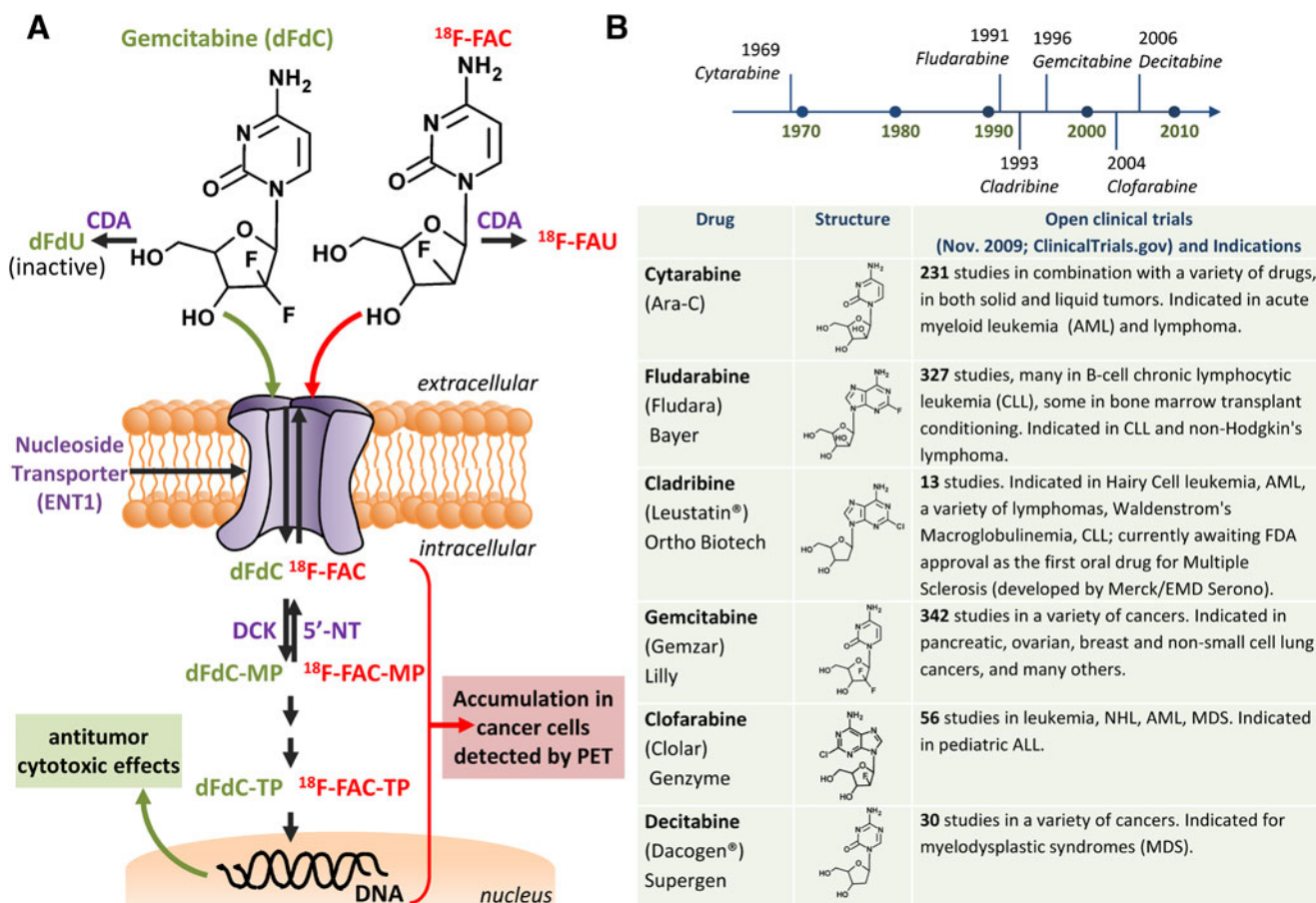
Fig. 1 **a** The dCK-dependent nucleoside analog prodrug gemcitabine (*dFdC*) and ^{18}F-FAC analogs share a common transport (*ENT1*) and phosphorylation (*dCK*) mechanism. Both gemcitabine and ^{18}F-FAC are subject to deamination by cytidine deaminase (*CDA*). *5'-NT* 5'-nucleotidase, *MP* monophosphate, *TP* triphosphate. **b** FDA-approved drugs that require dCK for their pharmacodynamic effects and the time line of their approval. Note the diversity of the chemical structures of these drugs, indicating the ability of dCK to phosphorylate both pyrimidine and purine analogs

PET acquisition

All volunteers fasted for at least 4 h before administration of the radiopharmaceutical. A whole-body ECAT/EXACT HR+positron emission tomograph (CTI/Siemens, Knoxville, TN, USA) was utilized [14]. The administered activity for each radiopharmaceutical was based on dosimetry studies in mice; the maximum allowed activity by the RDRC for ^{18}F-FAC was 407 MBq (11 mCi), for L-^{18}F-FAC 204 MBq (5.5 mCi), and for L-^{18}F-FMAC 122 MBq (3.3 mCi). Probe toxicity was ruled out in rats by necropsy after injecting the cold analogs at 100-fold higher concentrations than the radiolabeled analogs. ^{18}F-FAC was injected at an activity of 304±86 MBq (median 263; range 247–403 MBq), L-^{18}F-FAC at 188±5 MBq (median 185; range 185.0–193.5 MBq), and L-^{18}F-FMAC at 107±2 MBq (median 106; range 105–108 MBq), respectively.

The PET imaging protocol consisted of a transmission scan and three emission scans (from base skull to mid-thigh) starting at approximately 21, 48, and 77 min after intravenous tracer administration. Emission scan and transmission scan duration was 4 min per bed position for a total of six or seven bed positions, depending on the height of the volunteer.

Image reconstruction

PET images were reconstructed using an iterative algorithm (ordered subset expectation maximization, 2 iterations, 8 subsets). A 6-mm Gaussian smooth was applied post reconstruction. The reconstructed axial slices were assembled into a volume set of the upper body, from which coronal and sagittal planes could be extracted.

Dosimetry

The Medical Internal Radiation Dose (MIRD) schema was followed for the calculation of the absorbed dose [15]. The

reader is referred to the "Appendix" for a more detailed description. The OLINDA/EXM (Organ Level Internal Dose Assessment Code, Vanderbilt University, 2003) program was used to estimate the absorbed dose [16]. All significant emissions for ^{18}F were used in the computations. Organ absorbed doses are determined by integration of all source-target combinations using standardized human phantoms; here we used the adult male or adult female.

Regions of interest were placed using a 50% isocontour of an organ on the first volume set of the body and included the entire organ. The regions were copied to the later acquired scans and activity concentration determined. For the urinary bladder, a 25% isocontour was used. Organ volumes for each volunteer were assumed to be constant over time, i.e., the same on each scan, with the exception of the bladder, for which the actual volume was determined on every scan.

Organ activity concentration was measured at different time points and was not decay corrected. Organ mass was estimated to be a fraction of body weight as given in Table A.1 on p. 15 of ICRP publication 53 [17] and by OLINDA/EXM [16]. Measured activity concentration multiplied by organ mass yields total organ activity, i.e., accumulated activity at a specific time point. Organ activity was measured as a function of time.

Regions were drawn over the heart, kidneys, liver, marrow (spine), muscles (deltoid and trapezius), salivary glands, spleen, and urinary bladder. The scans did not include the upper part of the head. Since the probes do not cross the blood-brain barrier, cerebral uptake does not contribute to internally absorbed dose. No scans of the lower extremities were obtained; activity concentration for muscle and bone marrow were measured in the upper body and assumed to be the same for the legs. The entire bone marrow and muscle mass was included to calculate accumulated activity.

For most organs the probe uptake is rapid, and instantaneous uptake was assumed for our calculations. This initial uptake was obtained by extrapolation of the measured organ activity to the zero time point by assuming a linear function. This corresponds to Fig. 5 on p. 11 of the MIRD primer for absorbed dose calculations [15]. After the last measured point it was assumed that the activity remained in the organ and decayed with the physical half-life of ^{18}F. For the bladder a different time-activity curve was hypothesized. At time zero the bladder activity is zero, which increased linearly to the first measured time point. After the last time point, it was assumed that bladder contents remained the same with physical decay only. The measured organ curves were supplemented with the assumed early instantaneous uptake (linear increase for the urinary bladder; see MIRD primer Fig. 3 on p. 10 [15]) and hypothesized late decay, and interpolated over equidis-

tant time intervals (see "Appendix" Fig. A1). Numerical integration provided the area under the curve (see "Appendix" Fig. A2; MIRD primer Fig. 6 p. 12 [15]). Dividing this area under the curve, i.e., accumulated activity [15] or time-integrated activity (MIRD pamphlet 21 [18]), by the administered activity yields the residence time. The remainder of the body was estimated by subtracting the activity in the organs from the total body. The residence times were entered into OLINDA/EXM and the absorbed doses calculated. Absorbed doses were estimated for each volunteer separately. After applying the tissue weighting factors from ICRP publication 103 to the equivalent dose for each organ, the effective dose was obtained [19]. Gender averaging yielded the effective dose E for the reference person as explained in Fig. B.3 of ICRP publication 103 (p. 274) [19] (see "Appendix").

The assumption that all activity remained and decayed inside the organs after the last measured point is a conservative approach and may be considered as a "worst-case scenario." However, we did not aim for precise dosimetry, but conducted this study to ascertain that we were within RDRC limits for absorbed doses in human research.

Biodistribution

The activity concentration was decay corrected to the time of injection, so that the standardized uptake value (SUV) could be calculated. SUV is defined as: average organ activity in Bq/ml divided by average body activity (i.e., administered activity divided by body weight) in Bq/kg. A tissue density of 1 was assumed so that 1 ml corresponds to 1 g and the SUV becomes dimensionless. The SUV for several target tissues was computed for each time point. The biodistribution was visualized by creating maximum intensity projection images for rapid inspection.

For an in-depth discussion of SUV as a parameter having a "dimension" or being a simple ratio, the reader is referred to the Appendix of reference [20].

Results

A representative scan for each probe is given in Fig. 2 showing the highest activity in the bladder. Organ activity as a function of time was analyzed and biological half-life calculated using an exponential fit; the results are given in Table 1. Splenic uptake was high for ^{18}F-FAC but low for L-^{18}F-FAC and L-^{18}F-FMAC (Fig. 2). Some organs, such as muscle and liver, exhibited an actual increase in tracer uptake from 50 to 80 min after injection (indicated with a positive sign in Table 1). The vast majority of biological half-lives were longer than the physical half-life of ^{18}F.
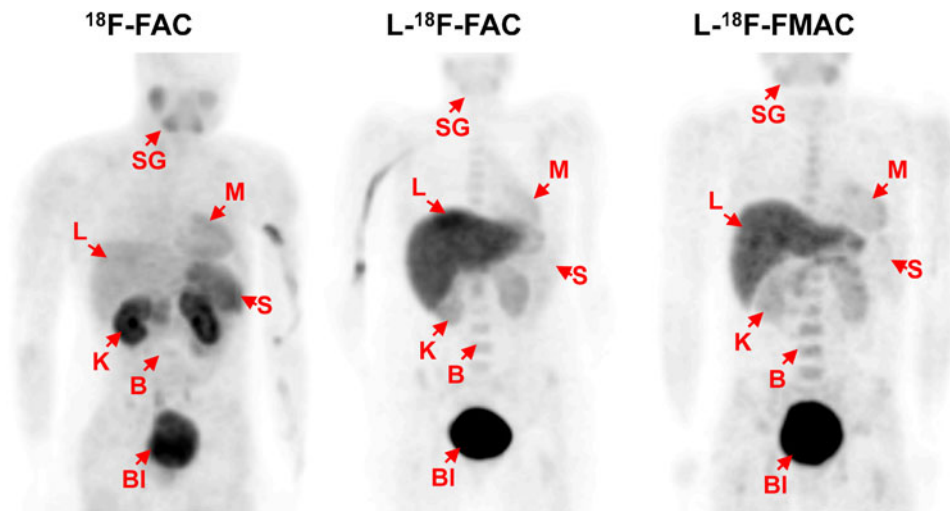
Fig. 2 Projection images obtained in three healthy volunteers using different FAC analogs. Organs are indicated by *arrows* (*B* bone marrow, *Bl* bladder, *K* kidney, *L* liver, *M* myocardium, *S* spleen, *SG* salivary gland). Note the high splenic uptake for ^{18}F-FAC while hepatic uptake was highest for L-^{18}F-FAC and L-^{18}F-FMAC. Bone marrow was visualized with all three tracers; marked tracer clearance is seen from kidneys into the bladder. The images are scaled to the maximum liver uptake, i.e., SUV 1.7 for the *left panel*, SUV 6.8 for the *middle panel*, and SUV 4.9 for the *right panel*; this permits direct comparison

The urinary bladder posed a particular problem. As expected, the activity increased with time. Of the nine volunteers, only three reached the maximum bladder uptake within 75 min. The other six had the maximum concentration on their third scan and the timing of the true maximum remains unknown. We assumed that the activity stayed within the bladder after the last measured time point and decayed completely with the physical half-life.

Dosimetry

The residence time τ was calculated for each probe and every volunteer by measuring the accumulated activity per organ and dividing it by the administered activity (see "Appendix"). The average τ per probe is given in Table 2 for various organs and the remainder of the body. The τs were the input for the OLINDA/EXM program, which then calculated the absorbed dose for each subject in the target organs. The critical organ (i.e., receiving the highest absorbed dose) for every probe was the bladder. Table 3 shows the highest absorbed dose per organ (i.e., the worst-case volunteer) for the particular probe. Administering an activity of 400 MBq would furnish an absorbed dose of 27 mGy to the bladder for L-^{18}F-FMAC. This worst-case scenario of no voiding is still within the allowed limit of 50 mSv (see "Appendix").

Average absorbed dose is shown in Table 4 for various organs and tissues. The organ receiving the highest absorbed dose was the bladder wall for all three probes. The spleen (for ^{18}F-FAC) and the liver (for L-^{18}F-FAC and L-^{18}F-FMAC) were second and the kidneys third (for all three probes).

The effective dose for the reference person as defined in ICRP publication 103 [19] (see "Appendix") is shown in Table 5. An administered activity of 400 MBq would result in an effective dose of 2.1±0.3, 3.0±0.5, and 3.6±0.7 mSv for ^{18}F-FAC, L-^{18}F-FAC, and L-^{18}F-FMAC, respectively. These values are well below the limit of 30 mSv as established in 21CFR361.1 [21] and applied by our RDRC for research in human subjects.

Biodistribution

The distribution of ^{18}F-FAC, L-^{18}F-FAC, and L-^{18}F-FMAC in the upper body of a typical healthy volunteer is shown in Fig. 2. High uptake in the bladder and kidneys was common to all three probes. Bone marrow was visualized

Table 1 Biological half-life in minutes for specific organs and probes. Mean±1 SD of three volunteers per probe

Organ	^{18}F-FAC	L-^{18}F-FAC	L-^{18}F-FMAC
Heart	−211±4	−292±94	−616±384
Kidneys	−107±9	−187±158	−112±68
Liver	−221±24	+516±370	+607±30
Marrow	−560±99	−733±99	−666±143
Muscle	+317±155	+918±1,853	+3,900±2,473
Salivary glands	−144±27	−340±325	+911±178
Spleen	−114±17	−343±281	−359±54

A plus sign indicates increasing uptake and a minus sign decreasing uptake with time

Urinary bladder is not measurable

Table 2 Residence time τ in hours. Mean±1 SD of three volunteers per probe

Organ	^{18}F-FAC	L-^{18}F-FAC	L-^{18}F-FMAC
Heart	0.0117±0.0010	0.0079±0.0019	0.0080±0.0007
Kidneys	0.0240±0.0033	0.0166±0.0019	0.0126±0.0043
Liver	0.0603±0.0060	0.1659±0.0454	0.1449±0.0295
Marrow	0.0235±0.0056	0.0328±0.0047	0.0232±0.0023
Muscle	0.4083±0.1002	0.2314±0.0043	0.2521±0.0199
Salivary glands	0.0035±0.0009	0.0029±0.0008	0.0029±0.0006
Spleen	0.0103±0.0012	0.0052±0.0030	0.0038±0.0004
Urinary bladder	0.0325±0.0047	0.0705±0.0104	0.1084±0.0121
Remainder	0.2787±0.1230	0.3365±0.2023	0.4000±0.1269

with all probes, with the lowest uptake for ^{18}F-FAC. L-^{18}F-FMAC and L-^{18}F-FAC exhibited a higher liver uptake than ^{18}F-FAC. Splenic activity was highest for ^{18}F-FAC, whereas the uptake for the other probes was low. Muscle uptake was higher for [18]-FAC than for the L-enantiomers.

The SUV averaged over three volunteers is displayed in Fig. 3 for several organs. The SUV for L-^{18}F-FMAC and L-^{18}F-FAC remained relatively stable during the observation period of about 100 min except for the myocardium and kidneys. In contrast, ^{18}F-FAC SUVs decreased in spleen and liver while muscle uptake increased slightly over time.

Discussion

The synthesis of ^{18}F-FAC, a deoxycytidine analog, was described previously [7, 8]. This probe is phosphorylated and trapped in tissues by dCK, a rate-limiting enzyme in the deoxyribonucleoside salvage pathway. ^{18}F-FAC shares a common biochemical pathway with a class of nucleoside prodrugs widely used in cancer therapy (Fig. 1). Both the imaging probe and these prodrugs are transported into the cells via equilibrative nucleoside transporters and are phosphorylated by dCK. The phosphorylation step is prerequisite to convert the inactive prodrugs into their active forms (reviewed in [6]).

The common metabolic fate of the probe and of the prodrugs suggests that ^{18}F-FAC could be used to predict treatment response. This was demonstrated in murine tumor models [8]. We found that ^{18}F-FAC accumulation was specific for dCK-positive tumors. Moreover, only the dCK-positive/^{18}F-FAC-positive but not the dCK-negative/^{18}F-FAC-negative tumors responded to gemcitabine treatment [8]. However, several of the dCK-dependent prodrugs (Fig. 1b) are deaminated by CDA to analogs that are not substrates for dCK, and therefore are pharmacologically inactive. Analogous to these prodrugs, ^{18}F-FAC is also deaminated, and this may decrease the amount of probe that can be trapped in dCK-expressing cells. Deamination could also increase background activity by producing ^{18}F-FAU, a radiolabeled metabolite of ^{18}F-FAC, in a dCK-independent manner.

On the prodrug side, the deamination issue has been solved by developing deamination-resistant purine analogs such as cladribine and clofarabine [22]. Since clofarabine is

Table 3 Highest individual absorbed dose per probe

Type	Organ	^{18}F-FAC	Organ	L-^{18}F-FAC	Organ	L-^{18}F-FMAC	Units
Volunteer							
Critical	Bladder	2.48E-02	Bladder	6.19E-02	Bladder	6.64E-02	mGy/MBq
2nd highest	Spleen	1.93E-02	Liver	4.31E-02	Liver	2.45E-02	mGy/MBq
3rd highest	Kidneys	1.86E-02	Kidneys	1.74E-02	Kidneys	1.67E-02	mGy/MBq
Patient							
Lymphoma	Bladder	6.4					mGy
	E	2.2					mSv
Ovarian cancer					Bladder	20.2[a]	mGy
					E	3.4[a]	mSv

E effective dose

[a] PET/CT study for which the RDRC and IRB have approved 370 MBq maximum administered activity

Table 4 Absorbed dose in mGy/MBq, three volunteers per probe, mean±1 SD

Target organ	^{18}F-FAC	L-^{18}F-FAC	L-^{18}F-FMAC
Adrenals	4.49E-03±8.96E-04	6.09E-03±1.70E-03	4.91E-03±8.64E-04
Brain	2.00E-03±7.59E-04	2.49E-03±1.34E-03	2.44E-03±7.00E-04
Breasts	2.23E-03±6.41E-04	2.82E-03±1.18E-03	2.53E-03±6.27E-04
Gallbladder wall	4.68E-03±7.79E-04	7.57E-03±2.07E-03	6.31E-03±1.22E-03
LLI wall	3.94E-03±8.05E-04	4.97E-03±1.58E-03	4.88E-03±8.43E-04
Small intestine	3.71E-03±8.00E-04	4.51E-03±1.47E-03	4.42E-03±8.93E-04
Stomach wall	3.72E-03±7.90E-04	4.47E-03±1.48E-03	3.86E-03±8.09E-04
ULI wall	3.76E-03±8.57E-04	4.91E-03±1.69E-03	4.42E-03±9.02E-04
Heart wall	9.71E-03±1.71E-03	9.12E-03±2.31E-03	7.27E-03±9.02E-04
Kidneys	1.77E-02±3.00E-03	1.45E-02±2.06E-03	1.07E-02±2.14E-03
Liver	9.96E-03±1.37E-03	2.84E-02±7.59E-03	1.93E-02±3.82E-03
Lungs	3.19E-03±7.40E-04	4.22E-03±1.40E-03	3.44E-03±7.41E-04
Muscle	4.83E-03±2.87E-04	4.72E-03±7.19E-04	3.84E-03±4.40E-04
Ovaries	4.09E-03±8.02E-04	5.11E-03±1.54E-03	4.96E-03±8.62E-04
Pancreas	4.59E-03±8.66E-04	5.88E-03±1.64E-03	4.86E-03±9.13E-04
Red marrow	4.56E-03±8.63E-04	5.61E-03±1.49E-03	4.86E-03±6.15E-04
Osteogenic cells	4.91E-03±1.49E-03	6.46E-03±2.32E-03	5.18E-03±1.03E-03
Skin	2.14E-03±5.01E-04	2.52E-03±9.91E-04	2.33E-03±5.20E-04
Spleen	1.37E-02±1.25E-03	9.24E-03±2.92E-03	6.21E-03±5.37E-04
Testes	2.83E-03±7.42E-04	a	3.64E-03±6.75E-04
Thymus	3.19E-03±6.81E-04	3.60E-03±1.36E-03	3.15E-03±6.87E-04
Thyroid	2.86E-03±5.40E-04	2.90E-03±1.20E-03	2.88E-03±6.49E-04
Urinary bladder wall	2.04E-02±3.95E-03	4.96E-02±7.22E-03	5.43E-02±6.03E-03
Uterus	4.59E-03±8.60E-04	6.28E-03±1.60E-03	6.77E-03±1.01E-03
Total body	4.20E-03±5.92E-04	4.97E-03±1.39E-03	4.32E-03±7.35E-04

LLI lower large intestine, *ULI* upper large intestine

[a] The volunteers for L-^{18}F-FAC were all female

amenable to ^{18}F labeling, in theory, ^{18}F-clofarabine could represent the solution to the deamination problem. However, we synthesized ^{18}F-clofarabine and found that this probe lacks the necessary specificity to image dCK-positive tissues in mice [11]. Therefore, we developed an alternative strategy to identify dCK substrates that are resistant to deamination. We took advantage of a special property of dCK. Unlike most enzymes, dCK lacks stereospecificity and acts on both natural (D-) and non-natural (L-) enantiomers of all its substrates [13]. In contrast, CDA is stereospecific and its affinity for non-natural nucleoside is greatly reduced [13]. Thus, we developed a series of L-enantiomers of ^{18}F-FAC for PET imaging of dCK activity. The radiochemical synthesis, biochemical evaluation, and biodistribution in mice of these new PET probes are described elsewhere [11].

Human biodistribution

Here we compared the biodistribution in humans of a D-enantiomer (^{18}F-FAC) and two L-enantiomers (L-^{18}F-FAC and L-^{18}F-FMAC). Based on the known pattern of dCK expression in tissues (reviewed in [3]) we expected these probes to show high uptake in hematopoietic/lymphoid tissues such as bone marrow and thymus.

The enzymatic activity of CDA, which is likely to affect the biodistribution of the radiolabeled D-enantiomers, also varies substantially among different species and organs [12]. In general, humans have more deamination activity than mice, while rats almost completely lack CDA activity. For instance, the ratio of dCK to CDA in murine splenic tissues is around 4:1, while it is 1:20 in the liver. In contrast, the

Table 5 Effective dose in mSv/MBq

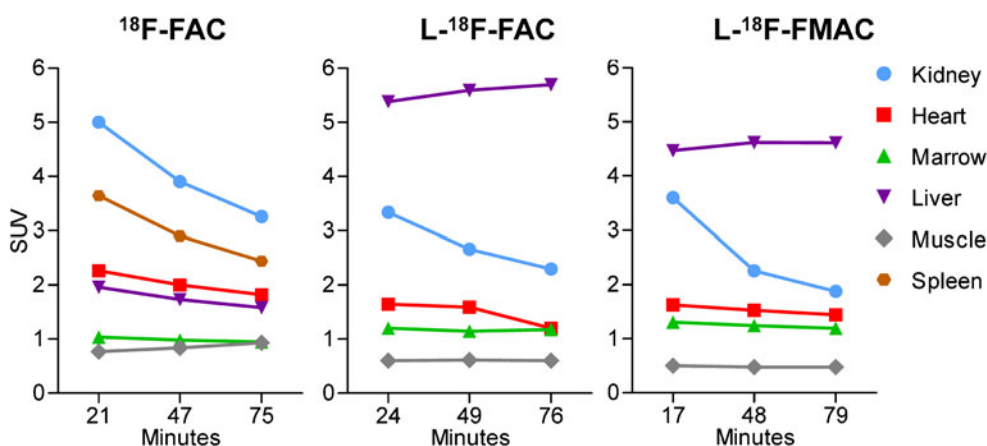| Type	Gender	^{18}F-FAC	Gender	L-^{18}F-FAC	Gender	L-^{18}F-FMAC
Volunteer 1	M	4.04E-03	F	9.69E-03	M	8.18E-03
Volunteer 2	M	5.54E-03	F	8.80E-03	M	6.40E-03
Volunteer 3	F	5.70E-03	F	6.14E-03	M	8.28E-03
Reference person		**5.24E-03**		**7.55E-03**		**9.10E-03**

Fig. 3 Dynamic changes in probe uptake; average of three volunteers per probe. Uptake is expressed as standardized uptake value (SUV$_{mean}$). ^{18}F-FAC activity in liver and spleen decreased over time while liver uptake of L-^{18}F-FAC and L-^{18}F-FMAC increased slightly. Bone marrow uptake was lowest for ^{18}F-FAC. Uptake is also noted in salivary glands and muscles (most prominently for ^{18}F-FAC)

ratio is around 1:20 in the human spleen and 1:200 in the human liver. Human bone marrow has very high CDA enzymatic activity, while this enzyme is essentially undetectable in the murine marrow [12].

None of the three PET probes showed thymic retention in our volunteers, which is not surprising since the involution of the thymus starts around puberty and is nearly complete by 30 years of age [23]. Future studies in patients with rebound thymic hyperplasia following chemotherapy will examine whether the thymus can be visualized using PET with fluorinated deoxycytidine analogs.

Fig. 4 ^{18}F-FAC images obtained in a patient with diffuse large B-cell lymphoma. The CT scan (*left panel*) shows extensive left axillary lymphadenopathy (*arrow*). This corresponds to a region of increased tracer uptake on the PET images suggesting that dCK expression of this lesion is high. *B* bone marrow, *Bl* bladder, *K* kidney, *L* liver, *LA* lymphadenopathy, *M* myocardium, *S* spleen. The scan was started 30 min after administration of 300 MBq of ^{18}F-FAC. See Table 3 for effective dose estimates

Bone marrow was well visualized with L-^{18}F-FAC and L-^{18}F-FMAC but less well with ^{18}F-FAC. The most likely explanation is that in humans ^{18}F-FAC undergoes extensive deamination in the blood and other organs and this significantly decreases the amount of probe available for trapping in bone marrow cells [12]. In contrast, splenic uptake was high for ^{18}F-FAC but at background levels for the L-enantiomers. Spleen and liver showed a significant decrease in activity for ^{18}F-FAC; the other organs did not show a significant change over the 100-min imaging period. This resulted in biological half-lives exceeding the physical half-life of ^{18}F (Table 1). PET imaging of dCK activity can be performed as early as 20 min after tracer injection.

High CDA levels are found in the human spleen and the splenic activity might therefore represent unspecific ^{18}F-FAU (the product of CDA-catalyzed deamination of ^{18}F-FAC) [12]. As shown in Fig. 3, the SUV of ^{18}F-FAC decreased over time and slopes of tracer clearance from the spleen resembled those from the kidneys. This suggests that the ^{18}F-FAC uptake in the spleen may not be dCK specific and that the high initial uptake might be explained by the high blood volume of this organ.

The D and L probes also differed in terms of liver uptake. Hepatic activity was higher for L-enantiomers than for ^{18}F-FAC. Uptake remained high and actually increased slightly during the imaging period (Fig. 3). In contrast, initial liver uptake of ^{18}F-FAC was about 60% lower and decreased further with time. Preliminary data obtained using a dCK-deficient mouse model [11] show a complete absence of L-^{18}F-FAC liver uptake. In contrast, wild-type mice show high liver uptake of L-^{18}F-FAC. These data suggest that, in mice and possibly in humans, the liver uptake is dCK specific. In this context, dCK is expressed in the human liver, albeit at lower levels than in bone marrow and thymus
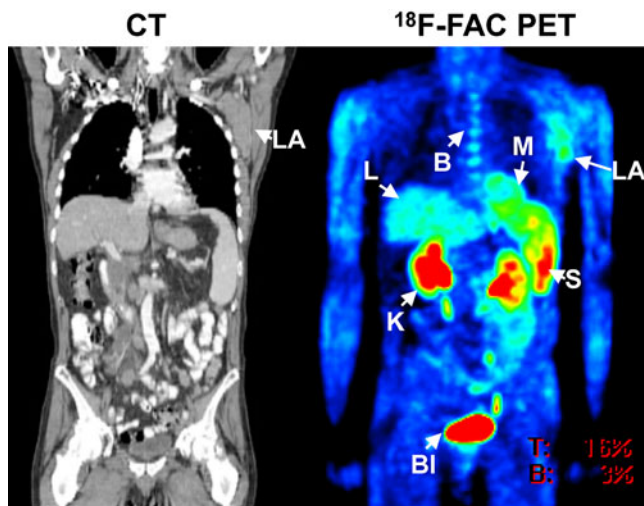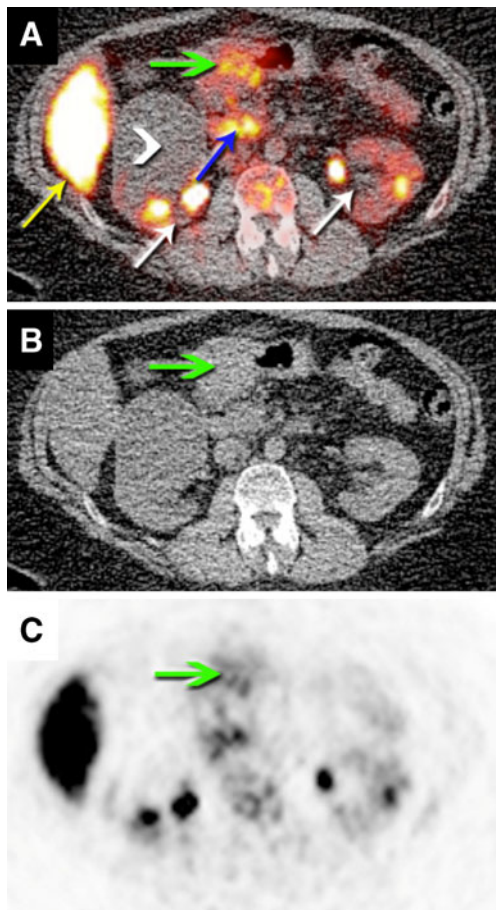
Fig. 5 Selected axial slices of PET/CT fusion (**a**), CT (**b**), and PET (**c**) obtained in a patient with metastatic ovarian cancer, demonstrating L-^{18}F-FMAC uptake in a metastatic lesion located in the gastric antrum. On PET/CT fusion images (**a**) physiologic uptake of L-^{18}F-FMAC is seen in the liver (*yellow arrow*) and pancreas (*blue arrow*); excreted L-^{18}F-FMAC is seen in both kidneys (*white arrows*). Incidental note is made of a large right renal cyst (*white arrowhead*). The scan was started 26 min after administration of 344 MBq of the radiopharmaceutical. Table 3 provides absorbed dose estimates

[12]. The lower hepatic uptake and the rapid "washout" of ^{18}F-FAC may be explained by differences in the transport of the natural and non-natural nucleoside analogs in hepatocytes.

Interestingly, the muscle uptake was markedly higher for ^{18}F-FAC than for the two L-enantiomers. This resulted in higher background activity for ^{18}F-FAC. For instance, bone marrow to muscle SUV ratio (muscle serving as background tissue) was close to 1 for ^{18}F-FAC but ranged from 2 to 3 for L-^{18}F-FAC and L-^{18}F-FMAC. A potential explanation for this observation is the rapid CDA-mediated conversion of ^{18}F-FAC to ^{18}F-FAU. The biodistribution of ^{18}F-FAU in humans has been studied by Sun and colleagues [24] who found that this PET probe has very slow blood clearance and relatively high muscle retention.

The biodistribution in a patient is shown in Fig. 4 for ^{18}F-FAC and in Fig. 5 for L-^{18}F-FMAC.

Radiation dosimetry

As shown in Tables 3, 4, and 5 the absorbed doses for the three probes are acceptable and favorable for research and clinical applications. For the two patients studied, the absorbed dose estimate of the urinary bladder and the effective dose are given in Table 3.

Assuming complete decay within the organs is conservative, since radioactivity can be excreted by an organ or be removed from the body altogether through the gastrointestinal (GI) or genitourinary (GU) tract. Despite this overly worst-case approach, the absorbed doses appeared to be well within the required limits [21]. The absorbed dose to the urinary bladder can be reduced significantly by frequent voiding. For the probe with the highest absorbed dose in the bladder, L-^{18}F-FMAC, the calculations were redone assuming 50% voiding of bladder contents every 2 h. This means that the effective half-life of tracer in the bladder is less than 1 h. OLINDA/EXM estimates revealed that the absorbed dose of the urinary bladder was reduced 15- to 24-fold, with a 7–22% decrease in the effective dose, E [19]. More realistic scenarios will also include different removal rates from certain organs (see Table 1) in addition to urinary voiding. These "real life scenarios" will reduce the absorbed dose even more, making the dosimetry of ^{18}F-labeled FAC probes more favorable than, for instance, ^{18}F-FDG with an effective dose of 1.9E-02 mSv/MBq (pp. 85–87 of ICRP publication 106 [25]).

Administering a dose of 400 MBq of an ^{18}F-labeled FAC probe is thus warranted for human research (Tables 3 and 5). It should be kept in mind that the calculation method used for patients in Table 3 is (unnecessarily) conservative. In clinical practice, patients are asked to void before they are positioned in the scanner. In addition, they are advised to drink ample fluids and void frequently after the scan. Thus, bladder emptying occurs and the actual absorbed organ and body doses will, in reality, be lower than estimated here.

Conclusion

The current studies confirm that ^{18}F-FAC, L-^{18}F-FAC, and L-^{18}F-FMAC have a favorable biodistribution in humans, and further evaluation of these new PET probes is warranted. Future studies will determine the ability of each of these probes to detect tumor lesions that have upregulated the dCK-dependent segment of the deoxyribonucleoside salvage pathway. The biodistribution of the D-enantiomer ^{18}F-FAC and the L-enantiomers L-^{18}F-FAC

and L-^{18}F-FMAC showed considerable differences for reasons which at this time are incompletely understood. Given the metabolic fate of ^{18}F-FAC, undergoing deamination by CDA, the L-enantiomers appear to be more promising for clinical use. Semiquantitative image analysis revealed higher background activity for ^{18}F-FAC than for the L-forms (Fig. 3). This reduces target to background ratios and henceforth image contrast. Despite its limited metabolic stability, ^{18}F-FAC might still be useful for clinical studies because of its low liver uptake. The first imaging study using ^{18}F-FAC in a patient with diffuse large B-cell lymphoma is depicted in Fig. 4. Increased tracer uptake in a large left axillary lymph node conglomerate is evident. Figure 5 shows the first patient study performed with L-^{18}F-FMAC showing a gastric metastasis of an ovarian cancer. Based on these promising results, we have initiated PET imaging studies in patients with a variety of solid tumors with the objective of identifying the most sensitive and specific deoxycytidine analog for measuring dCK activity in human cancers.

Conflicts of interest C.G.R., J.C., and O.N.W. are among the inventors of the national and PCT patent applications for the FAC technology referred to in the article. That patent application was filed on 19 September 2008. A group of UCLA faculty members including C.G.R., J.C., M.E.P., and O.N.W. are involved in Sofie Biosciences, a startup company that has licensed this intellectual property.

References

1. Weber W, Grosu A, Czernin J. Technology Insight: advances in molecular imaging and an appraisal of PET/CT scanning. Nat Clin Pract Oncol 2008;5:160–70.
2. Jemal A, Siegel R, Ward E, Hao Y, Xu J, Thun MJ. Cancer statistics, 2009. CA Cancer J Clin 2009;59:225–49.
3. Staub M, Eriksson S. The role of deoxycytidine kinase in DNA synthesis and nucleoside analog synthesis. In: Peters GJ, editor. Cancer drug discovery and development: deoxynucleoside analogs in cancer therapy. Totowa: Humana; 2006. p. 29–52.
4. Kulke MH, Tempero MA, Niedzwiecki D, Hollis DR, Kindler HL, Cusnir M, et al. Randomized phase II study of gemcitabine administered at a fixed dose rate or in combination with cisplatin, docetaxel, or irinotecan in patients with metastatic pancreatic cancer: CALGB 89904. J Clin Oncol 2009;27:5506–12. doi:10.1200/JCO.2009.22.1309.
5. Lilenbaum R, Villaflor VM, Langer C, O'Byrne K, O'Brien M, Ross HJ, et al. Single-agent versus combination chemotherapy in patients with advanced non-small cell lung cancer and a performance status of 2: prognostic factors and treatment selection based on two large randomized clinical trials. J Thorac Oncol 2009;4:869–74. doi:10.1097/JTO.0b013e3181a9a020.
6. Jordheim LP, Dumontet C. Review of recent studies on resistance to cytotoxic deoxynucleoside analogues. Biochim Biophys Acta 2007;1776:138–59. doi:10.1016/j.bbcan.2007.07.004.
7. Radu CG, Shu CJ, Nair-Gill E, Shelly SM, Barrio JR, Satyamurthy N, et al. Molecular imaging of lymphoid organs and immune activation by positron emission tomography with a new [18F]-labeled 2'-deoxycytidine analog. Nat Med 2008;14:783–8.
8. Laing RE, Walter MA, Campbell DO, Herschman HR, Satyamurthy N, Phelps ME, et al. Noninvasive prediction of tumor responses to gemcitabine using positron emission tomography. Proc Natl Acad Sci U S A 2009;106:2847–52.
9. Ewald B, Sampath D, Plunkett W. Nucleoside analogs: molecular mechanisms signaling cell death. Oncogene 2008;27:6522–37. doi:10.1038/onc.2008.316.
10. Gandhi V, Plunkett W. Clofarabine and nelarabine: two new purine nucleoside analogs. Curr Opin Oncol 2006;18:584–90. doi:10.1097/01.cco.0000245326.65152.af00001622-200611000-00007.
11. Shu CJ, Campbell DO, Lee JT, Tran AQ, Wengrod JC, Witte ON, et al. Novel PET probes specific for deoxycytidine kinase. J Nucl Med 2010;51:1092–8. doi:10.2967/jnumed.109.073361.
12. Ho DH. Distribution of kinase and deaminase of 1-beta-D-arabinofuranosylcytosine in tissues of man and mouse. Cancer Res 1973;33:2816–20.
13. Maury G. The enantioselectivity of enzymes involved in current antiviral therapy using nucleoside analogues: a new strategy? Antivir Chem Chemother 2000;11:165–89.
14. Wienhard K, Dahlbom M, Eriksson L, Michel C, Bruckbauer T, Pietrzyk U, et al. The ECAT EXACT HR: performance of a new high resolution positron scanner. J Comput Assist Tomogr 1994;18:110–8.
15. Loevinger R, Budinger TF, Watson EE, Society of Nuclear Medicine (1953-). Medical Internal Radiation Dose Committee. MIRD primer for absorbed dose calculations (revised edition). New York: Society of Nuclear Medicine; 1991.
16. Stabin MG, Sparks RB, Crowe E. OLINDA/EXM: the second-generation personal computer software for internal dose assessment in nuclear medicine. J Nucl Med 2005;46:1023–7. doi:46/6/1023.
17. ICRP. Radiation dose to patients from radiopharmaceuticals. ICRP Publication 53. Approved by the Commission in March 1987. Elmsford: Pergamon; 1988.
18. Bolch WE, Eckerman KF, Sgouros G, Thomas SR. MIRD pamphlet No. 21: a generalized schema for radiopharmaceutical dosimetry—standardization of nomenclature. J Nucl Med 2009;50:477–84 doi:10.2967/jnumed.108.056036.
19. ICRP. The 2007 Recommendations of the International Commission on Radiological Protection. ICRP publication 103. Ann ICRP 2007;37:1–332. doi:10.1016/j.icrp.2007.10.003.
20. Schiepers C, Hoh CK, Nuyts J, Seltzer M, Wu C, Huang SC, et al. 1-11C-acetate kinetics of prostate cancer. J Nucl Med 2008;49:206–15. doi:10.2967/jnumed.107.044453.

21. FDA. 21CFR361 - Code of Federal Regulations Title 21 Part 361 Section 1. HHS; 1975 (revised April 1, 2010).

22. Jeha S, Gandhi V, Chan KW, McDonald L, Ramirez I, Madden R, et al. Clofarabine, a novel nucleoside analog, is active in pediatric patients with advanced leukemia. Blood 2004;103:784–9. doi:10.1182/blood-2003-06-2122.

23. Taub DD, Longo DL. Insights into thymic aging and regeneration. Immunol Rev 2005;205:72–93. doi:10.1111/j.0105-2896.2005.00275.x.

24. Sun H, Collins JM, Mangner TJ, Muzik O, Shields AF. Imaging the pharmacokinetics of [F-18]FAU in patients with tumors: PET studies. Cancer Chemother Pharmacol 2006;57:343–8. doi:10.1007/s00280-005-0037-0.

25. ICRP. Radiation dose to patients from radiopharmaceuticals. Addendum 3 to ICRP Publication 53. ICRP Publication 106. Approved by the Commission in October 2007. Ann ICRP 2008;38:1–197. doi:10.1016/j.icrp.2008.08.003.